ISRN LUTMDN/TMHP—10/5220—SE
ISSN 0282-1990

Water wheel CFD simulations

Ali Al Sam

Thesis for the Degree of Master of Science

Division of Fluid Mechanics
Department of Energy Sciences
Faculty of Engineering
Lund University

Water Wheel CFD Simulations

Ali Al Sam

Thesis for the Degree of Master of Science

Division of Fluid Mechanics
Department of Energy Sciences
Faculty of engineering, LTH
Lund University
P.O. Box 118
SE-221 00 Lund
Sweden

Abstract

Water wheel is non-polluting electricity generation plants that harness the energy available in natural water sources. A channeling device is added to the water wheel to concentrate the flows energy into the turbine.

Calculations of a number of different blade and channeling device geometries have carried out by using the commercial computational fluid dynamic software Fluent.

Sliding mesh model were used to compare different numbers and types of blades.

The calculations shows that 10.5kw shaft power with about 0.66 power coefficient can be produced by using 4m diameter water wheel .

Acknowledgments

This thesis carried out in cooperation between Ideon Science Park, Lund and the Department of Energy Sciences at Lund Institute of technology.

I would like to thank Johan Revstedt who has supervised this thesis work.

In ideational I would to thank all friends who performing their thesis work in fluid department in parallel to mine, for the discussion and all good time we spent.

Lund, October 2010

Ali Al Sam

1. Introduction

One of the greatest challenges in this century is to produce sufficient energy. The Increase in world population and the continuous economical growth in many countries require more access to energy. The U.S.A department of energy DOE projects global energy demand to increase by 20% by 2025[2].

The decreasing in coal and oil resources and the global warming problem creates an increasing need for sustainable alternative energy resources. Hydropower forms 95% of the worldwide produced sustainable energy and about 20% of the world's electricity overall [1].

1.1 Objective

The mean objective of this thesis is to carry out calculations for a number of different geometry for a new type of low speed water wheel using the commercial computational fluid dynamic software Fluent.

This new waterwheel is designed for usage in the countryside of developing countries at sites remote from the existing electricity grid. The water wheel designed by Ideon to have a horizontal axis and run at a low velocity. The waterwheel is placed between two curved hydrofoils which have the task to concentrate the flows energy into the turbine. The wheel should have a small geometry to reduce the initial and operation costs. Figs 1-2 show the proposed water wheel and channeling device.

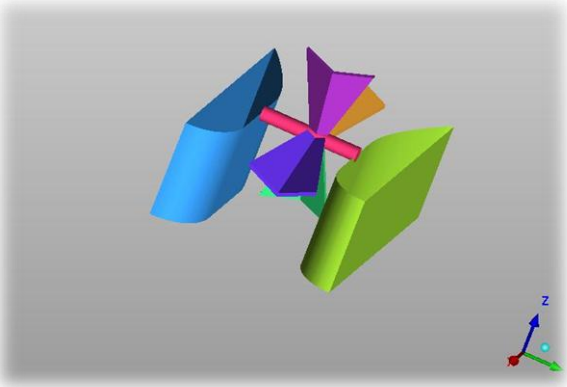

Figure 1.1 water wheel

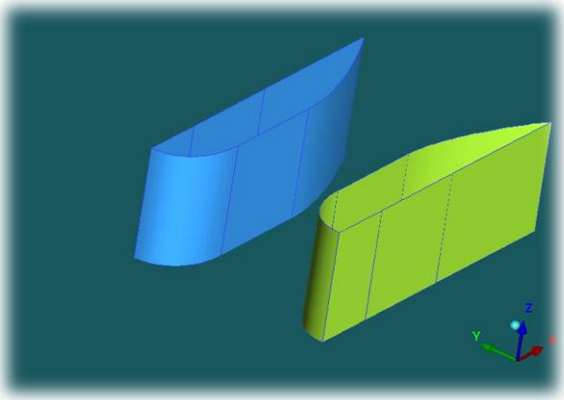

Figure 1.2 channeling device

The aims of this study are to investigate the performance of channeling device and to calculate the efficiency and the expected shaft power from this water wheel. The study compares between the suggested triangular blades with blades have rectangular shape. The calculated shaft power from water wheel has four blades compares with one has six blades.

1.2 Short history of hydraulic turbine

Greeks used waterwheel to crush grapes for wine and grinding grain for bread. In the thirteenth century Chinese engineers used tidal power of the waves to crush iron ore. Leonardo Da Vinci designed a wave machine in the fifteenth century. The first commercially successful hydraulic turbine was developed by Benoit about 1830. A radial-inflow hydraulic turbine was designed by Francis. In the second half of nineteenth century Pelton introduced his wheel turbine. In 1913 Kalpan revealed his idea of a propeller turbine [3].

1.3 Water turbine classification

Water turbines are usually classified according to the concept of work generation, into either impulse or reaction turbines. In reaction turbines the difference in pressure across the blade produce lift forces cause the runner to rotate. This type of turbine should be totally immersed in the water and enclosed in a casing.

Impulse turbines are rotated by the force created by the change in velocity direction of the flow, which causes a change in momentum [4]. This change of momentum causes forces on the turbine blades. Impulse turbines do not required to be immersed in the flow since there is no change in pressure in the fluid surrounding the turbine blades.

Reaction Turbines	Impulse Turbine
Francis Kalpan Tyson, Gorlov Archimedean screw turbine	Pelton Turgo Banki-Michell turbine

Table 1.1 classifications of water turbines

Hydro-kinetic turbines produce electricity from the flowing water in a river. The most common small scale turbine concepts are axial flow turbines and cross flow [4]. In axial turbines the axis of rotation is parallel to the incoming water stream, this category also include inclined axis propeller, submerged and non submerged turbines. The cross-flow turbine has a rotational axis parallel to water surface [4]. The cross flow turbines can be divided into vertical axis and in plane axis.

Vertical axis turbine has its axis of rotational vertical to the water plane. There are many different turbines using this concept [4], such as H-Darrieus, Squirrel cage Darrieus, Gorlov, Savonious.

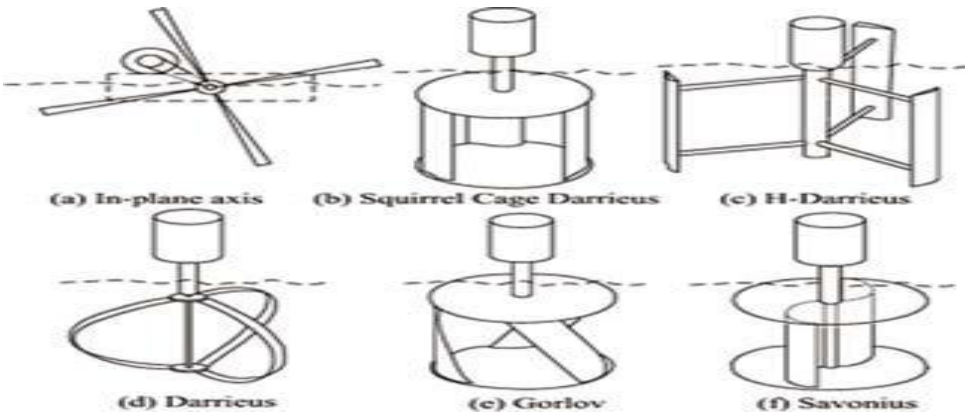

Figure 1.3 Types of water turbines [3]

The disadvantages associated with this type of turbine are its low starting torque and low efficiency. In-plane axis turbines have an axis on horizontal plane of water surface. This type of water turbine is known also as floating water wheels. The in- plane turbines are mainly drag based devices (the blade speed is less than the water speed) and is said to be less efficient than lift turbines(blade faster than the water[4].

2. Governing equations for fluid flow

Fluid flow analyzed by means of conservations laws: conservation of mass, conservation of momentum and conservation of energy.

2.1 Conservation of mass

The law of mass conservation, which also is known as the continuity equation states that the rate of increase of mass inside an element is equal to the net flow rate of mass into the element across its faces. The integral equation for the conservation of mass [7]:

$$\int_{\vartheta} \frac{\partial \rho}{\partial t} \partial \vartheta + \int_{s} \rho (\underline{V} \times \underline{n}) ds = 0$$

Eq-2.1

Where the first integral corresponds to the control volume and the second one corresponds to the boundary surface of the control volume. For the steady state case the first term is eliminated. In case of incompressible flow where the density variation is small and can be neglected and if the steady state one-dimensional flow assumptions are valid, the above equation can be written as

$$V_{in} A_{in} = V_{out} A_{out} = Q$$

Eq-2.2

Where V and A are the velocity and the cross section area respectively, and Q is the volumetric flow rate.

2.2 Conservation of energy

The equation of energy conservation is a direct application of the first law of thermodynamics and states that the net rate of heat added plus the net rate of work done equal the time rate of energy change in the control volume. The conservation of energy equation can be written in different forms. For flow in open channel the integral equation for the conservation of energy can be written as:

$$Q_c - W = \int_{\vartheta} \frac{\partial}{\partial t} \rho \left(\frac{V^2}{2} + u + gy \right) d\vartheta + \int_{s} \rho \left(\frac{V^2}{2} + u + gy + \frac{P}{\rho} \right) (\underline{V} \times \underline{n}) ds$$

Eq-2.3

For adiabatic, isothermal and without mechanical work interchange with the surrounding medium, the two terms in left side of the above equation will disappear.

2.3 Conservation of momentum

The governing equation for momentum is based on Newton's second law which relates the fluid particle acceleration to the sum of forces acting on a fluid particle,

$$\sum F_{\substack{contents\ of\ the \\ control\ volume}} = \frac{\partial}{\partial t}\int_{cv} V\rho d\vartheta + \sum V_{out}\rho_{out}A_{out}V_{out} - \sum V_{in}\rho_{in}A_{in}V_{in}$$

Eq-2.4

The forces that can act on fluid particle are either body forces or surface forces. The forces that classify as body forces are: gravity forces, centrifugal forces, Coriolis forces and electromagnetic forces. While the surface forces are the pressure forces and viscous forces.

By considering only the gravity forces as a body forces and neglecting all other forces and by expressing the surface forces by its equivalent stress tensor the Navier-Stokes equation for incompressible, Newtonian fluid can be written [7] as

$$\rho\frac{Du_j}{Dt} = \mu\frac{\partial^2 u_j}{\partial u_j \partial u_i} - \frac{\partial p}{\partial x_i} + \rho g_i$$

Eq-2.5

The three components of Navier-Stokes equation when combined with the conservation of mass equation provide a complete mathematical description of the flow of incompressible, Newtonian fluids.

3. Open channel flow

Open channels can either be artificial channels made by man as in irrigation channels or natural channels as in rivers. Unlike artificial channels which usually have known geometry the natural channels' geometries are varied. The variation of geometry and surface roughness in natural channels makes it difficult to predict the flow characteristics accurately. However this thesis is only concerned with artificial channels with regular cross section.

Types of flow in open channel [9]:

- Steady: the flow depth at a particular point can be considered constant for the time interval under consideration. If it changes the flow is said to be unsteady.
- Uniform flow: the depth and velocity of the flow are constant at every section of the channel.
- Steady non-uniform: depth varies with distance but constant with time.
- Unsteady flow: varies with both time and space.

The drive force in open channels is the gravity force which makes it different from flow in pipes for example which is driven by pressure work [9]. The other difference from flow in pipes is the free surface which's position is not known beforehand. Because of the existence of this free surface in open channel the flow depth become variable along the channel which adds difficulties to flow analyses.

By assuming the fluid to be inviscid, the fluid motion is governed by pressure and gravity forces only. If the density and the specific weight are constant and the flow is steady along the streamlines, then the Bernoulli equation is valid [7]

$$p + \frac{1}{2}\rho V^2 + \gamma z = constant\ along\ streamlin$$

Eq-3.1

By divided each term in Bernoulli equation by the specific weight the summation of elevation, pressure and velocity heads become constant along the stream line

$$\frac{p}{\gamma} + \frac{v^2}{2g} + z = constant$$

Eq-3.2

Where $\frac{p}{\gamma}$ represent the pressure head, $\frac{v^2}{2g}$ $the\ velocity\ head$ and z is the elevation head. By considering the frictional losses a new terms should be added to eq-3.2

$$\frac{p_1}{\gamma} + \frac{v_1^2}{2g} + z_1 = \frac{p_2}{\gamma} + \frac{v_2^2}{2g} + z_2 + h_l$$

Eq-3.3

$z_1 = z_2$ Vertical distance from a datum

$\frac{p}{\gamma}$ Is hydrostatic pressure those it can be replaced by flow depth y.

4. Turbine efficiency

The power available from water can be determined from equation

$$P_{available} = 0.5 \times A_w \times \rho \times V^3$$

Eq-4.1

A_w : Cross section area under consideration.

The water wheel converts part of this power to a shaft power [10]

$$P_{shaft} = 0.5 \times C_p \times A_{wheeel} \times \rho \times V^3$$

Eq-4.2

Where C_p is the power coefficient of the wheel and represents the ratio between the power output from the wheel and power available in the water. Not all of the available power is converted to shaft power by the wheel. Leaving water should have sufficient kinetic energy to continue its way outside the wheel. The above equations show that the power output from the wheel depends on the available power and the efficiency of the wheel.

If the velocity vectors assumed to be parallel to each other, the approach velocity is equal to velocity inlet V_{in} minus the runner velocity $(V_{in} - u)$ where u is runner velocity $(u = R\Omega)$. If the water recedes from blade in the opposite direction of the incoming water and if the friction losses are neglected the outlet velocity become [-$(V_{in} - u)$+u] =$[-V_{in} + 2u]$

In the ideal case all kinetic energy on the water can be converted to shaft power so the velocity of receding water equals zero [3]. That mean the optimal case reached when u equal to half of V_{in}.

To study the performance of water wheel at different incoming velocities, the wheel velocity is normalized by the incoming velocity and a non-dimensional parameter called tip speed ratio is defines as [10]

$$\lambda = \frac{u}{V_{in}} = \frac{R\Omega}{V_{in}}$$

Eq-4.3

According to Newton's second law the force on the blades of the wheel equal the rate of momentum change of the fluid [3]

$$F = -\rho Q\,[(-V_i + 2u) - V_i] = -\rho Q\,(-2V_i + 2u) = 2\rho Q\,(V_i - u)$$

Eq-4.4

The shaft torque $\tau \; is \; equal \; to \; F \times R$ so that

$$\tau = \rho Q R \, (V_i - u)$$

Eq-4.5

Max torque is obtained when wheel is stopped and u=0 , while the torque becomes zero when the wheel has the same velocity as the water.

At a fixed geometry and fixed inlet conditions the wheel efficiency(or the power coefficient) increase as the tip speed ratio increase until a certain point where the efficiency is maximum and then gradually starts to decrease as the tip speed ratio is further increased [3].

5. Turbulent

Turbulence is a flow characteristic in which the viscous forces are small compared to the inertia forces. In turbulent flow the viscous force has no ability to damp out small perturbations in boundary and initial condition, instead these p44erturbations are amplified causing rapid variation in pressure and velocity in space and time. The criterion for determining which forces are dominate, the inertia or viscous forces is the Reynolds number

$$Re_{channel} = \frac{\rho u R}{\mu}$$

Eq-6.1

Where R is the hydraulic radius (cross section area divided by wetted parameter).

For open channel there is no clearly limit at which Re the turbulence developed in flow but it usually taken as Re =2000. So for flow in open channels, the flow is rarely laminar since the viscosity of water is in order of 10^{-3} and its density is of the order 10^{3} which will give Re in order of10^{6}

The random and chaotic variations in the flows' variables make it impossible to predict the instantaneous value of dependent variables. Instead a static description used to solve turbulent flow problems. The velocity is decomposed into a steady mean value and fluctuation part.

$$U = \overline{U} + u$$

Eq-6.2

Where U is the instantaneous velocity, $\overline{U}$ mean velocity and u is the fluctuation component.

Solving the continuity and momentum equation for the mean velocity the result will be the mean-momentum or Reynolds equation [6]

$$\frac{\overline{D}}{\overline{Dt}}\overline{U_J} = \frac{\partial}{\partial x_i}\left[v_{eff}\left(\frac{\partial \overline{U_i}}{\partial x_j} + \frac{\partial \overline{U_J}}{\partial x_i}\right) - \frac{1}{\rho}\overline{P}\delta_{ij} - \overline{u_i u_J}\right]$$

Eq-6.3

Reynolds equations differs from the Navier-Stokes equations in 6 terms which are called Reynolds stresses $\boldsymbol{\partial u_i u_j}$

In general three-dimensional flow there are four independent equation governing the flow, the continuity equation and 3 Reynolds equations in three directions. In these four equations there are seven unknowns, three components of the mean velocity, three components of Reynolds stresses and the mean pressure. According to the turbulent-viscosity hypothesis which was introduced by Boussinesq, the deviatoric Reynolds stress is proportional to the mean rate of strain. The scalar

coefficient v_t is called turbulent viscosity. By introducing this turbulent viscosity the Reynolds equation written as [6]

$$\frac{\overline{D}}{\overline{Dt}}\overline{U}_J = \frac{\partial}{\partial x_i}\left[v_{eff}\left(\frac{\partial \overline{U}_i}{\partial x_j} + \frac{\partial \overline{U}_J}{\partial x_i}\right)\right] - \frac{1}{\rho}\frac{\partial}{\partial x_j}\left(\bar{P} + \frac{2}{3}\rho k\right)$$

Where $v_{eff}(\boldsymbol{X}, t) = \nu + v_t(\boldsymbol{X}, t)$

The above equation is similar to Navier-Stokes equation in form and to solve it the turbulent viscosity have to be modeled.

This thesis is not intends to study the validity of different turbulent models, therefore the focus will be only on describing the model used in this thesis. Due to limitation in time and computational sources, an advance and complex turbulent model can't be use in this thesis which aims to study the flow around rotating part with large computational domain and relatively large mesh scale. Two equation models give an acceptable accuracy with reasonable time and resource consumption therefore they are used in this thesis.

In two equation model two turbulence quantities are solved, for example in k-ε model the turbulence kinetic and turbulence dissipation are solved to obtain the necessary length and time scale to calculate turbulent viscosity [8].

$$L = k^{2/3}/\epsilon$$

Eq-6.4

and

$$\tau = k/_{\epsilon}$$

Eq-6.5

Stander k-epsilon model solve one equation for k and other one for epsilon, while in k-ω models, one equation solve for k and the second one can be one of those quantities ω, ω^2 or τ [8].

K-ε model is the simplest complete model and one of the most widely used models. The reasonable accuracy and low computational requirement make it so attractive model. The stander K-ε model uses empirical value for c_μ which is used to calculate the turbulent viscosity from k and ε

$$v_\tau = \rho C_\mu \, k^2/_{\epsilon}$$

Eq-6.6

The value of c_μ calculated from measuring $\frac{\overline{u_i u_j}}{k} = 0.3$ when production equal to dissipation of the turbulent. $\frac{\overline{u_i u_j}}{k} = (C_\mu \frac{\mathbb{P}}{\epsilon})^{1/2}$, where $\mathbb{P}$ represent the production in this relation [8].

The K equation in k- ϵ model [8]:

$$\frac{\partial}{\partial t}(\rho k) + \frac{\partial}{\partial x_i}(\rho k u_i) = \frac{\partial}{\partial x_j}\left[(\mu + \frac{\mu_t}{\sigma_k})\frac{\partial k}{\partial x_j}\right] + G_k + G_b - \rho\epsilon - Y_M + S_k$$

Eq-6.7

And for ϵ

$$\frac{\partial}{\partial t}(\rho\epsilon) + \frac{\partial}{\partial x_i}(\rho\epsilon u_i) = \frac{\partial}{\partial x_j}\left[(\mu + \frac{\mu_t}{\sigma_\epsilon})\frac{\partial \epsilon}{\partial x_j}\right] + G_{1\epsilon}\frac{\epsilon}{k}(G_k + C_{3\epsilon}G_b) - C_{2\epsilon}\rho\frac{\epsilon^2}{k} + S_\epsilon$$

Eq-6.8

G_k generation of turbulent due to the mean velocity gradients

G_b generation of turbulent due to buoyancy

Y_M Fluctuating dilation in compressible turbulence to the overall dissipation rate

σ_k turbulent Prandtl number for k and have a value of 1

σ_ϵ turbulent Prandtl number for ϵ and have a value of 1.3

$G_{1\epsilon}$, $C_{2\epsilon}$, constants $G_{1\epsilon} = 1.44$, $C_{2\epsilon} = 1.92$,

In stander k-ϵ model the k equation drive directly from the exact equation, while ϵ equation is empirical.

Many of standard k-ϵ models features enhanced during the time and its application expand to cover a lot of engineering problems. One of recently development model of k-ϵ model is the realizable k-ϵ model. In Realizable k-ϵ model ϵ equation has been derived from the exact equation for the mean-square velocity so both of k and ϵare driven from the exact equation. In addition to new ϵ equation the realizable model has a new formulation for turbulent kinetic viscosity [8]

The impact of this change in k-ϵ model is increasing of its accuracy and better performance to deal with flow involving rotation, adverse pressure gradients.

Realized k-ϵ model doesn't use a constant value for C_μ but it calculates it from mean flow.

The realized k-ϵ model equations are [8]:-

$$\frac{\partial}{\partial t}(\rho k) + \frac{\partial}{\partial x_i}(\rho k u_i) = \frac{\partial}{\partial x_j}\left[(\mu + \frac{\mu_t}{\sigma_k})\frac{\partial k}{\partial x_j}\right] + G_k + G_b - \rho\epsilon - Y_M + S_k$$

Eq-6.8

$$\frac{\partial}{\partial t}(\rho\epsilon) + \frac{\partial}{\partial x_i}(\rho\epsilon u_j) = \frac{\partial}{\partial x_j}\left[(\mu + \frac{\mu_t}{\sigma_\epsilon})\frac{\partial \epsilon}{\partial x_j}\right] + \rho C_1 S_\epsilon - \rho C_2\frac{\epsilon^2}{k + \sqrt{\upsilon\epsilon}\epsilon} + C_{1\epsilon}\frac{\epsilon}{k}C_{3\epsilon}G_b + S_\epsilon$$

Eq-6.9

Where $C_1 = max\left[0.43, \frac{\eta}{\eta+5}\right]$, $\eta = S\frac{k}{\epsilon}$, $S = \sqrt{2S_{ij}S_{ij}}$

This model show a better performance than the stander k-ϵ model or RNG-K-ϵ model when it deals with anisotropic turbulence especially at high Re and cases that include body forces as in rotating cases. Because of these features in the standard k-ϵ model it was used in this study.

The k-ϵ models are designed to solve the turbulent far from the wall therefore near wall treatment have to be add. The near wall region is divided into three layers; viscous sub layer where the viscosity is dominate and flow behavior as a laminar flow, the fully- turbulence layer at the outer layer where the turbulence is dominate and the buffer layer between those two layer where both the effect of both turbulence and viscosity are important.

Standard wall functions solve the logarithmic law for mean velocity for a range of $30 < y^* < 300$ but in fluid the log-law applied when $y^* > 11.225$ while when y^* has a value less than 11.225 the mean velocity give a value equal to y^* $U^* = y^*$ (when $y^* < 11.225$)

Where the log-law $U^* = \frac{1}{\kappa}Ln(EU^*)$ and $y^* = \frac{\rho C_\mu^{1/4} k_p^{1/2} yp}{\mu}$

K is a Von Karman constant 0.4187

E empirical constant 9.793

k_p turbulent kinetic energy at the near wall node p

y_p distance from point p to the wall

The standard near wall function has its limitation when the flow has a strong body force. In this case the near wall model should combine with adequate mesh resolution. Enhanced wall function can be used for such cases. Enhanced wall function provides a single law for those three layers near the wall.

6. Methods

There is no analytical solution for the governing equations presented in chapter 2 therefore numerical methods should be used to solve these equations. The commercial software fluent uses Finite volume method to solve fluid flow problems by using computer-based simulation.

6.1 Finite Volume Method

In Finite volume method the domain is subdivided into number of control volumes (cells). Flows' variables are located at the center of cells. The integral forms of governing equations are applied to each cell. For each control volume the value at faces are by interpolation [15]

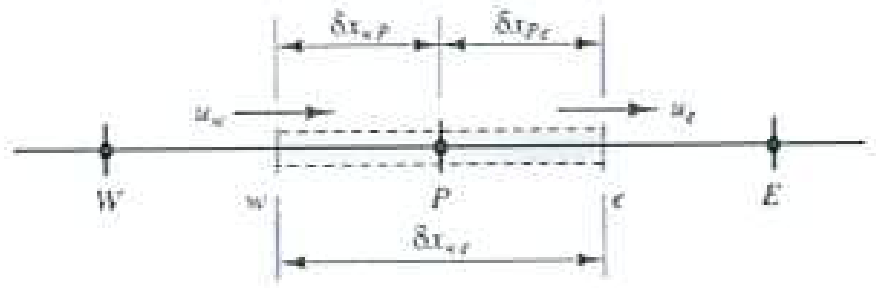

Figure 6.1 the control volume in FVM

The general form of transport equation can be write as

$$\frac{\partial(\rho\varphi)}{\partial t}+\frac{\partial}{\partial x}(\rho u_i\varphi)=\frac{\partial}{\partial x_i}(\Gamma\frac{\partial\varphi}{\partial x_i})+S$$

Eq-6.1

Where φ an arbitrary scalar, Γ is the diffusion coefficient and s is source term.

The first term in eq 6.1 is the transient term, $\frac{\partial}{\partial x}(\rho u_i\varphi)$ is the convection term and $\frac{\partial}{\partial x_i}(\Gamma\frac{\partial\varphi}{\partial x_i})$ is the diffusion term.

To calculate the transported property at the control volumes faces different scheme are used:

- Central difference scheme
- Upwind scheme $\varphi_e=\varphi_P$and
- Hybrid
- QUICK (Quadratic Upwind Interpolation for Convection Kinetics)
  For example the center difference method solve the transported property at faces as $\varphi_e=\frac{\varphi_E-\varphi_p}{2}$ while upwind solves it as $\varphi_e=\varphi_P$and $\varphi_{w=}\varphi_W$.

6.2 pressure-velocity coupling

In the discretised form of governing equation there is a linear dependence of velocity on pressure and vice.-versa. There are four equations (3 momentum and 1 continuity) to solve the three components of velocity and the pressure, but the continuity equation cannot be used directly to obtain the pressure. A special treatment is required. The methods used to solve this problem can be classified into [16]:

- Staggered methods in which the velocities are stored at grid points faces while other scalar variables are stored at the centers of control volumes.
- Non staggered methods in which all variables are stored in the centers of control volumes but a special interpolation (Rhie-chow) method used to calculate velocity components at the cell faces.

Examples of staggered methods:

SIMPLE (Semi-Implicit Method for Pressure-Linked Equation)

SIMPLEC (Semi-Implicit Method for Pressure-linked Equations, consistent)

SIMPLER (Semi-Implicit Method for Pressure-Linked Equations, Revised)

SIMPLEX (Semi-Implicit Method for Pressure-Linked Equations, eXtrapolation)

PISO (pressure implicit with splitting of Operators)

SIMPLE scheme was used in this thesis.

6.3 Rotating and sliding mesh

In Fluent there are three models that can be used to solve fluid flow problems around rotating or moving parts. They are rotating reference frame, multiply reference frame and sliding mesh.

In rotating reference frame the equations of motion are modified to be solved in rotating reference frame instead of a stationary reference frame. The equations are solved as steady state with respect to the rotating reference frame. By transforming the coordinates from stationary to moving reference frame an additional acceleration terms should be added. These terms are added automatically by fluent when moving reference frame is selected.

To solve the equations of motion in rotating reference frame either the relative velocity between the stationary and rotating frame used as a dependent variable in momentum equations or the absolute velocity.

The relation between the stationary and rotating velocity is:

$$\overrightarrow{v_r} = \vec{v} - \overrightarrow{u_r}$$

Eq-6.2

Where

$$\overrightarrow{u_r} = \vec{w} \times \vec{r}$$

Eq-6.3

Where $\overrightarrow{v_r}$ is the relative velocity, $\vec{v}$ is the absolute velocity and $\vec{w}$ is the whirl velocity.

$\vec{r}$ is the position vector from an arbitrary point in rotating domain to the origin of the rotating [14]

If relative velocity is used to solve the moving equations, the governing equations become

Continuity:

$$\frac{\partial \rho}{\partial t} + \nabla . \rho \overrightarrow{v_r} = 0$$

Eq-6.4

Momentum

$$\frac{\partial}{\partial t}(\rho \vec{v}_r) + \nabla . (\rho \vec{v}_r \vec{v}_r) + \rho(2\vec{w} \times \vec{v}_r + \vec{w} \times \vec{w} \times \vec{r}) = -\nabla p + \nabla . \bar{\bar{\tau}}_r + \vec{F}$$

Eq-6.5

Where $\bar{\bar{\tau}}_r$, is the viscous stress and $\vec{F}$ is a body forces.

The two terms in the right hand side is the Coriolis acceleration $2\vec{w} \times \vec{v}_r$ and centripetal acceleration $\vec{w} \times \vec{w} \times \vec{r}$

While if absolute velocity is used as the dependent variable the equation become [14]:

$$\frac{\partial \rho}{\partial t} + \nabla . \rho \overrightarrow{v_r} = 0$$

Eq-6.6

$$\frac{\partial}{\partial t}(\rho \vec{v}) + \nabla . (\rho \vec{v}_r \vec{v}) + \rho(\vec{w} \times \vec{v}) = -\nabla p + \nabla . \bar{\bar{\tau}}_r + \vec{F}$$

Eq-6.7

In the cases that involve only one moving zone, Single reference frame SRF model can be used. In SRF model all parts in the domain should have the same velocity and the same axis.

For the cases that involve more than one moving zone or parts that move in different velocity or rotate around different axis's multiple cell zones should be used. There are two steady state

approximations to treat the interface between zones, either by using multiply reference frame MRF or mixing plane.

MRF, which is also known as the frozen rotor approach, is the simplest and less computationally heavy of the multiple zones approaches. In this model the equations of motion are solved with respect to a separate rotating reference frame for each zone. Since the velocity and velocity gradients change with a change in reference frame special treatment should be applied. At the boundary between two sub domains the program enforces the continuity of the absolute velocity to provide the correct neighbor values of velocity for each sub domain [14]. While in case of using relative velocity with MRF the velocity and velocity gradients are convert from the moving reference frame to stationary frame by using the equation bellow:

$$\vec{v} = \vec{v}_r + (\vec{w} \times \vec{r}) \times \vec{v}_t$$

Eq-6.8

Flow variables at the interface are used to solve fluxes at the adjacent zone by transferring the reference frame locally over the two sides of the interface. This approximation doesn't solve the relative velocity between adjacent cell zones and only gives instantaneous steady state solution of rotating parts at a specific position. MRF is useful approximation to many problems and is also used to predict the initial flow for the transient sliding mesh.

In the mixing plane approximation the flow equations are also solved as steady state with respect to a moving reference frame. The only difference between mixing plane and MRF is that the flow field data from adjacent zones are averaged at the mixing planes to provide the information about the coupling between two adjacent zones. This data can be averaged by using one of three different ways; area weighted averaging, mass averaging and mixed-out averaging. After a specific number of iterations decided by the user, the flow data will have converged to an averaged at the interface. Specific boundary condition should be defined for the interface at each cell zone in the domain in a manner so that the upstream outlet is coupled with the downstream inlet into a mixing plain pair. The creating of the mixing plane require one of the following pair of boundary conditions:-pressure outlet-pressure inlet, pressure outlet-velocity inlet, and pressure outlet-mass flow inlet.

The only unsteady model in fluent that can handle the flow around a rotating or moving part is the sliding mesh. In sliding mesh the relative motion is solved between adjacent zones. The sliding mesh model is the most accurate model that deals with moving or rotating reference frame.

With sliding mesh the integral form of the conservation equation on a moving control volume V written as

$$\frac{dy}{dx}\int_V \rho\phi dV + \int_{\partial V} \rho\phi(\vec{u} - \vec{u}_g).d\vec{A} = \int_{\partial V} \Gamma\nabla\phi.d\vec{A} + \int_V S_\phi dV$$

Eq-6.9

Where $\vec{u}\ is\ the$ flow velocity vector, $\vec{u}_g$ is the mesh velocity of the moving mesh, S_ϕ is a source term.

The first term desecrates as follow [14]

$$\frac{dy}{dx}\int_V \rho\phi dV = \frac{(\rho\phi V)^{n+1} - (\rho\phi V)^n}{\Delta t}$$

Eq-6.10

The volume at n+1 time level is compute from

$$V^{n+1} = V^n + \frac{dV}{dt}\Delta t$$

Eq-6.11

Mesh conservation requires that

$$\frac{dV}{dt} = \int_{\partial v} \overrightarrow{u_g}.d\vec{A} = \sum_j^{nf} \vec{u}_{gj}.\vec{A}_j$$

Eq-6.12

Where nf is the number of faces on the control volume $\vec{A}_j$ is the face area vector. The dot product of mesh velocity and faces area is equal to the swept volume out by the control volume face j over the time step

$$\overrightarrow{u_g}.d\vec{A} = \frac{\delta V_j}{\delta t}$$

Eq-6.13

In sliding mesh the control volume remains constant therefore $\frac{dV}{dt} = 0$ and equation 6.10 can be written as:

$$\frac{dy}{dx}\int_V \rho\phi dV = \frac{[(\rho\phi)^{n+1} - (\rho\phi)^n]}{\Delta t}$$

Eq-6.14

6.4 Assumptions

Due to the complicated nature of open channel flows such as the flow in rivers, many assumptions and simplifications must be made.

The geometry is assumed to be uniform along the channel and the depth of the channel is constant i.e. steady uniform open channel flow.

The flow is assumed to be clean water without sediments, at constant temperature and properties (998.2 kg/m^3density and 0.001003 kg/ms viscosity)

The effect of free surface on the velocity profile is neglected and the free surface is defined as solid wall with slip condition.

Constant flow discharge which mean constant inlet velocity.

A constant velocity profile is given in the inlet. The walls effect on inlet velocity profile are neglected since they are far away from the area under consideration(10m from the inlet and 15m from the side walls) that will give the flow enough time to fully develop.

6.5 problem approach

Channeling device was studied first .Both two dimensions and three dimensions cases were studied to select the channel geometry. Two types of blades were compared by using stationary mesh.

Sliding mesh approach was used to study the shaft output power from water wheel by trying two types of blades for two different blade numbers.

The channeling device consists of three parts. A nozzle to concentrate flow energy into rotor zone is followed by a straight channel to get uniform flow into the rotor and finally a diffuser to readjust the outlet channel flow with the river flow. To find smallest geometry for channeling device that can give good effect, a number of geometrical parameter have been studied.

- Length of channeling device C to the width of the river w c/w.
- Width of the straight channel to the river width x/w
- Hydrofoil max thickness to its length t/c

The geometry of hydrofoils was generated depending on NACA symmetrical airfoil series. The airfoil is cut at the point of max thickness and the straight channel is imposed between the two parts of the hydrofoil.

The two dimensional geometry was studied first. Block method was used to generate structural grid. The first cell distance from solid is located at 0.001m from solid boundary. The grid density at channel area was double as much as other domain with gradually decrease to avoid high aspect ratio. The quality of mesh was checked by ICEM tools .The converged results of 2D steady state case were compared to select the best geometry. One parameter changed each time and fixed all other parameters.

The numerical results compared with theoretical results which calculated from

$$V_{in}A_{in} = V_{channel}A_{channel}$$

Eq-6.15

A_{in} is the nozzle inlet width, $A_{channel}$ is the straight channel width.

In numerical results $V_{channel}$ was calculated by integral velocity values along the straight channel's width.

$$V_{channel} = \frac{\int V \, dA}{A}$$

Eq-6.16

Channel device is studied also in three dimensional. Computational domain was generated by extend the 2d geometry in z direction. Unstructured tetrahedral mesh was used in the three dimensions cases with prismatic layers around the hydrofoils. The tetrahedral unstructured mesh advantages is to reduce the total number of used cell by using appropriate cell size and shape where it is required and coarse mesh in the less important area. However the unstructured mesh has its disadvantage since it produce more numerical diffusion comparing with structural mesh.

Two types of blade were studied, triangular and rectangular, see figure below. The main part of this project was to study the possibility of using triangular blade and expected increase of efficiency arising from the use of this type of blade. Its dimension and shape was suggested by Ideon. This new types of blade was compared with rectangular blade which has uniform shape.

Using report forces features in fluent to calculate the torque component parallel to incoming water produced by blades around wheel shaft.

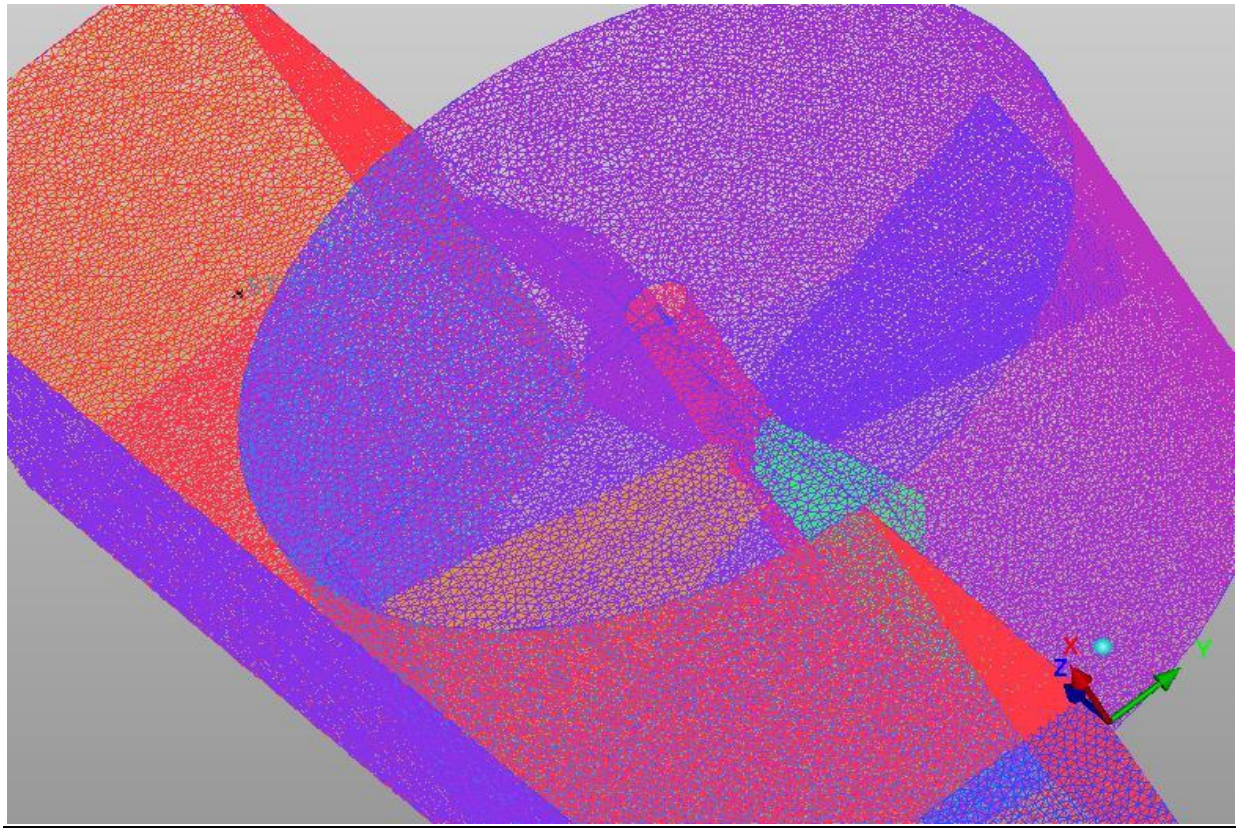

Figure 6.2 Unstructured mesh

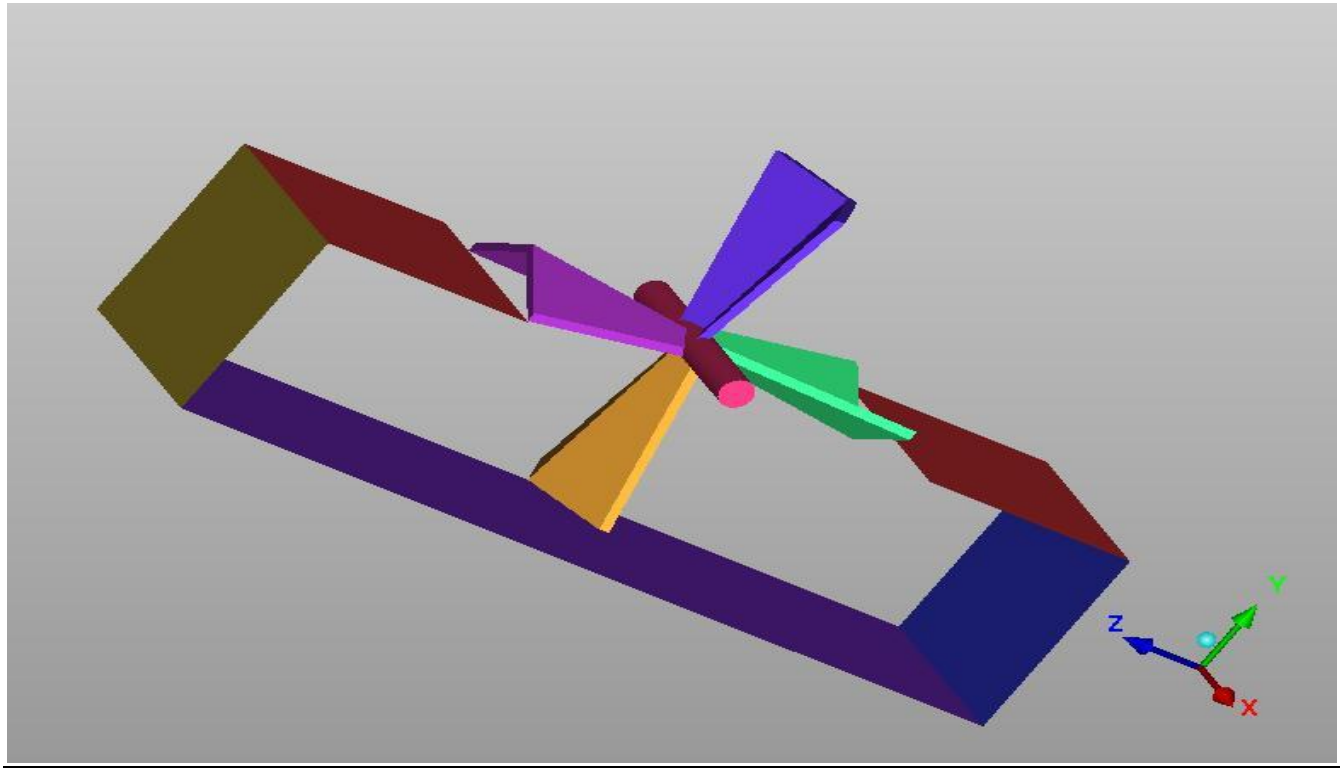

Figure 6.3 Four triangular blades

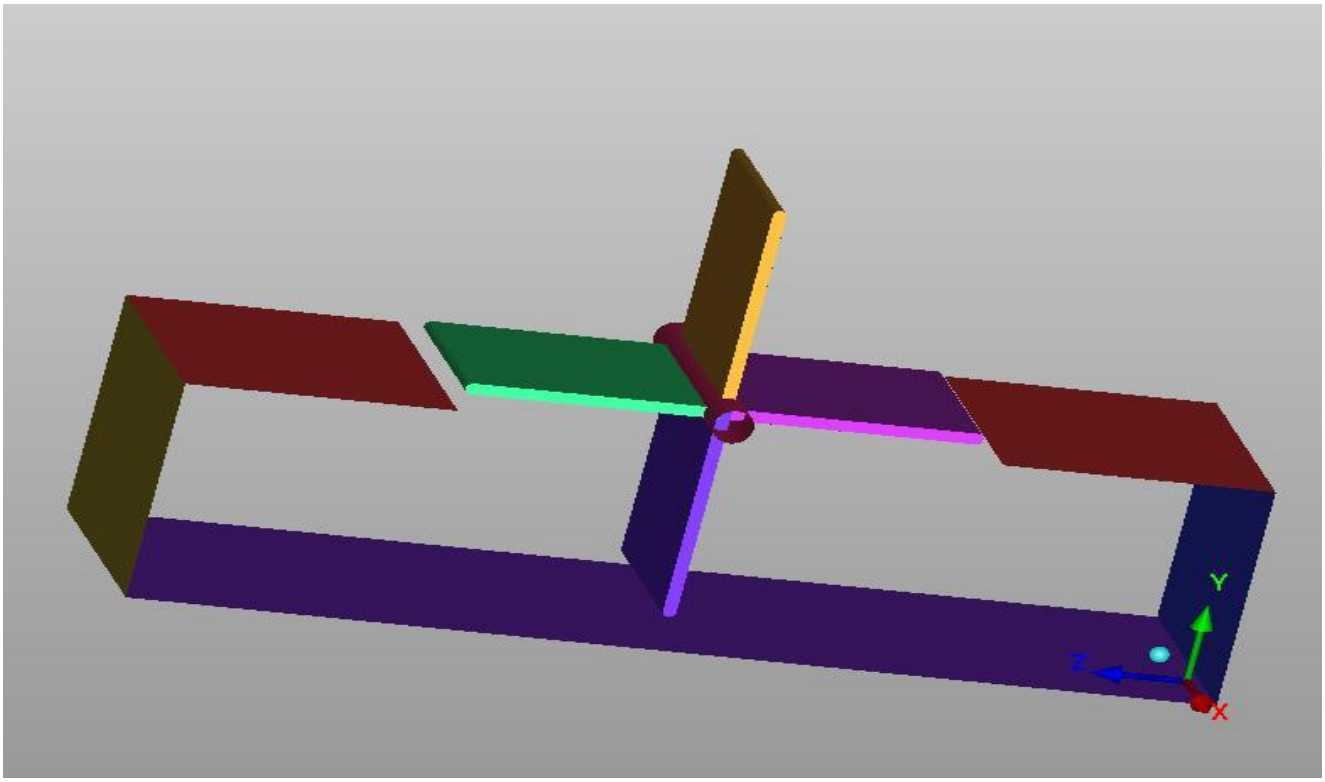

Figure 6.3 Four triangular blades

7. Cases setting

7.1 Channeling device

Two dimensional (30m×30m) computational domain was used in all 2D cases. Residual of value 10^{-6} residual criteria were given to all equations. Default under relaxations values was also used. Turbulent intensity of 4% and 0.14m length scale were given to turbulent field in all cases. The flow initialized from inlet boundary conditions.

7.1.1 2D cases

- **Mesh and turbulent model selection**
  The cell numbers and turbulent model are studied for a specific geometry (t/c=6%, X=2m, c=4m). The boundary conditions used in this part explained by table 7.1

Geometry	Inlet	outlet	Hydrofoils	Side walls
B.C	Velocity inlet	Outflow	No slip wall	No slip walls
Value	1.5m/s	1*		

Table 7.1 mesh and turbulent selection cases boundary conditions set up
*Flow rate weighting value.

Studied cases are summarized in following table:

grid	k-epsilon	Wall function
100,000	Standard	Standard
200,000	Standard	Standard
250,000	Standard	Standard
200,000	RNG	Standard
200,000	Realized	Standard

Table7.2 mesh and turbulent model set up

- **Hydrofoil width to its length ratio**

  Number of cases with different Hydrofoil width to length ratio was carried out. Total length of channeling device was fixed at 6m, the straight channel dimensions were 2m width and 2m length. 200,000 cells were used. First cell putted at 0.001 m from the solid boundary and 5 layers were used with expansion ratio of 1.1. Standard k-epsilon model with standard wall treatment was used in this part. 1.5m constant inlet velocity was given to all cases.
- **Straight channel width**
  Hydrofoils with 22% thickness to length ratio were used to study the straight channel width. Five different ratios between the widths of straight channel to river width were studied. Inlet velocity was constant in all cases with value of 1.5m/s
- **Total length of the channel**
  By keeping the t/c ratio at 44% and straight channel with fixed dimensions (2m×2m), three different lengths were studied. No other change in setting was made.
- **Channeling performance at different inlet velocity**

The channel device was studied at different inlet velocity. 6m length channel with 44%width to length ratio and (2m×2m) straight channel was used. All other settings were the same as above section.

7.1.2 3D cases3D

Computational domain (30m×30m×2m) was used. The domain was meshed by using about 900,000 tetrahedral with maximum cell length of 0.05m. Five layer of prismatic mesh were used around the hydrofoils. K-epsilon model with standard wall treatment were used. The under relaxation factor was reduced to 0.3 value for all equations. In 3D cases gravity field in –z direction was added. Three cases with three different inlet velocities (1m/s, 2m/s, 2.5 m/s) were studied.

7.2 Rotor and blades

To study the shaft power of the water wheel, Realizable k-epsilon turbulent model with enhanced wall treatment were used. Second order accuracy discratization was used for all terms. Under relaxation factor for pressure was reduced to 0.2 and for other variable to 0.3 values.

7.2.1 Stationary blades

The computational domain was box, 3m length, 2m width and 2m height, with stationary blade fixed in the middle of it. Two types of blade were studied and compared, triangular and rectangular. Blades were studied at three different angles with respect to incoming fluid (45deg, 90deg, 135deg).

2m/s constant inlet velocity was used as inlet B.C., out flow for outlet and no slip condition for all walls and hydrofoils except the upper surface which given slip boundary condition.

Steady state, double precision, pressured based model was used with Realizable k-epsilon and enhanced wall treatment was used. SIMPLE scheme for pressure-velocity coupling was also used.

7.2.2 Sliding Mesh

8m long computational domain with 2m width and 2m height was used in sliding mesh. The domain consists of two zones, stationary and moving. Moving wall with zero relative velocity with respect to adjacent zone was given to the blade, shaft and moving zone side walls. Interface surfaces between the stationary and moving zones were defined as interface.

Incompressible, Unsteady state, double precision, pressured based model was used with Realizable k-epsilon and enhanced wall treatment was used. SIMPLE scheme for pressure-velocity coupling was also used.

Implicit scheme with 10^{-2}s time step and 20 iterations per each time step was used in all sliding cases. The moments around the shaft were written in a file for each blade at each time step by Fluent.

Number of mesh cells varied from case to case depending on blades number and types but it was about 1.2 million cells in all cases.

7.2.2.1 Four triangular blades

Four triangular blades studied first for five different tip speed ratio (0.2, 0.4, 0.5, 0.6, 0.7, 0.8, and 1). Depending on tip speed ratio different rotating speed were given to rotational zone. Inlet velocity kept constant at 2m/s value.

One case studied with 3m/s inlet velocity and 1.05 rps angular velocity (i.e. 0.7 tip speed ratio) to compare with other case have the same tip speed ratio.

7.2.2.2 Four rectangular blades

Same set up as in triangular blade was used to study wheel with 4 rectangular blades at three different tip speed ratio (0.5, 0.7, 0.8) with constant 2m/s inlet velocity.

7.2.2.3 Six rectangular blades

Six blades wheel was studied using the same set up for four blade wheel with same boundary conditions for 0.7 tip speed ratio and 2m/s inlet velocity.

8. Results and discussions

A number of geometrical parameters were studied. In most 2D cases the results differ slightly from the theoretical calculations.

The channeling cases include stream line curvature. This curvature has two effects in turbulent field, first to increase the length scale and second effect is to increase the anisotropy. So the deviation from the theoretical result was expected by using k-epsilon turbulent model which build on the assumption that the Reynolds stress anisotropy part is determined at any point and time from mean velocity gradient.

The realizable k-epsilon model showed a slight difference from standard k-epsilon model and it needs almost three times as many iterations to converge.

The number of cells in the channel area was enough to solve the flow with acceptable accuracy.

The results of mesh and turbulent model study are summarized in table 8.1

grid	k-epsilon	V channel
100,000	Standard	2.328
200,000	Standard	2.498
250,000	Standard	2.4978
200,000	RNG	2.52
200,000	Realized	2.496

Table 8.1 Mesh and turbulent model results

The channeling length and straight channel width results are introduced in table 8.2 and 8.3 respectively.

C/w	6/30	8/30	10/30
Theoretical	2,82	3.48	4.14
Numerical	2,7082	3,443	4,0268

Table 8.2 Total channel length to river width ratio

X/w	5/30	4/30	3/30	2/30	1/30
Theoretical	2,028	2,16	2,38	2,82	4,14
Numerical	1.98	2,0952	2,844	2,7082	3,937

Table 8.3 straight channel width to river width ratio

The hydrofoil thickness study showed how the velocity of straight channel increases by increasing the thickness to chord ratio. At 22% t/c ratio the flow has a maximum velocity. When the hydrofoils curvature was increased they lost their ability to direct the fluid along its curvature. Enlarged contour plots show the difference in velocity profiles for 8% and 24%.

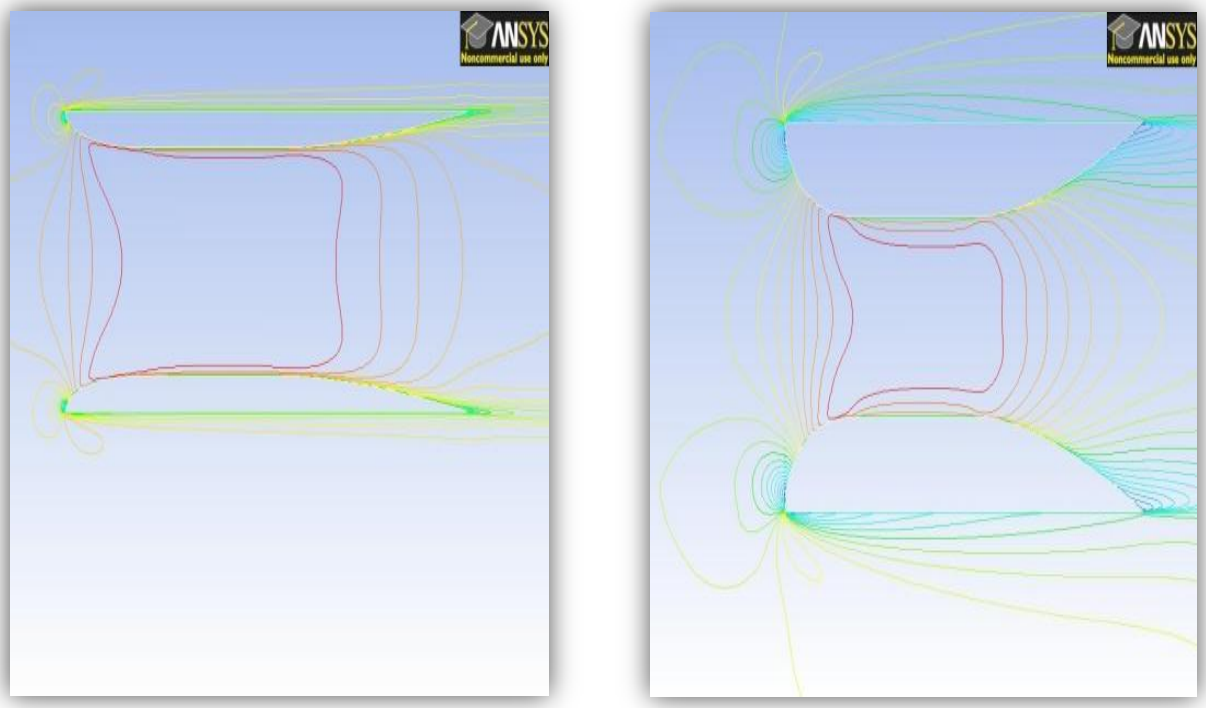

Figure 8.1 velocity profiles for 8%t/c (left) and 22% t/c(right) hydrofoils.

Table 8.4 shows the effect of hydrofoil thickness on flow velocity.

t/c	6%	8%	10%	12%	14%	16%	18%	20%	22%	24%
Theoretical	2,48	2,64	2,8	2,96	3,12	3,28	3,44	3,6	3,76	3,92
Numerical	2.498	2.654	2.806	2.95	3.091	3.196	3,311	3,405	3,472	3,358

Table 8.4 hydrofoil thickness to its length ratio

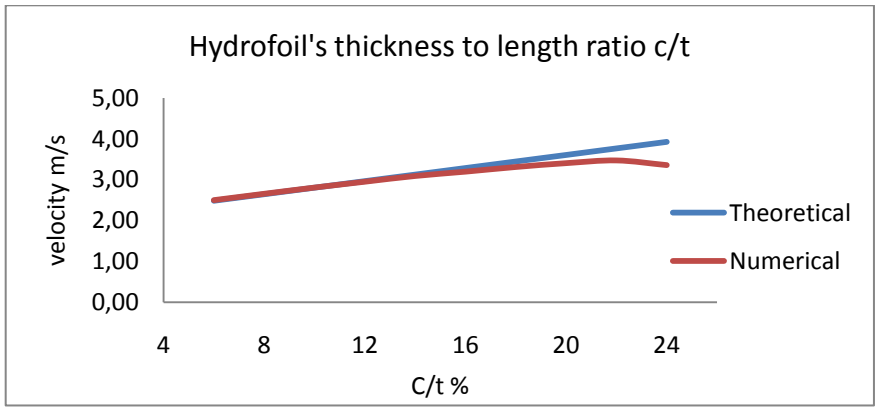

Figure 8.2 Hydrofoil's thickness to length ratio

By increasing the inlet velocity the channel velocity is also increased. It's clear from both theoretical and numerical values that the increase in velocity is less than theoretical curve. The theoretical

values were derived by assuming parallel stream lines and one directional velocity. In reality the flow in channel is far away from being parallel. High turbulent intensity noticed at the channel inlet. This turbulent intensity increases when velocity increases due to increasing in Re.

V_{inlet}	1	1.1	1.2	1.3	1.4	1.5	1.6	1.7	1.8	1.9	2
Theoretical	1.88	2.068	2.256	2.444	2.632	2.82	3.008	3.196	3.384	3.572	3.76
Numerical	1.822	1.971	2.127	2.289	2.454	2.621	2.789	2.958	3.128	3.299	3.472

Table 8.5 channel performance at different inlet velocities

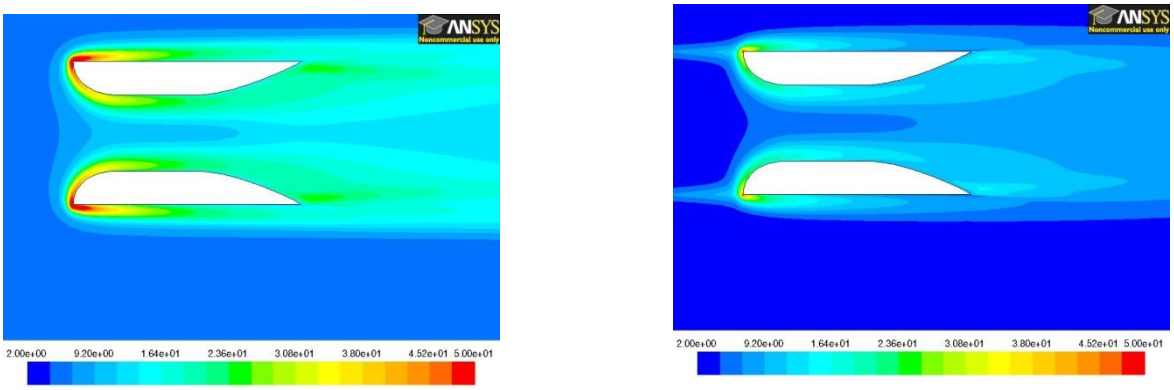

Figure 8.3 turbulence intensities, 1.9m/s inlet velocity left and 1 m/s velocity inlet right.

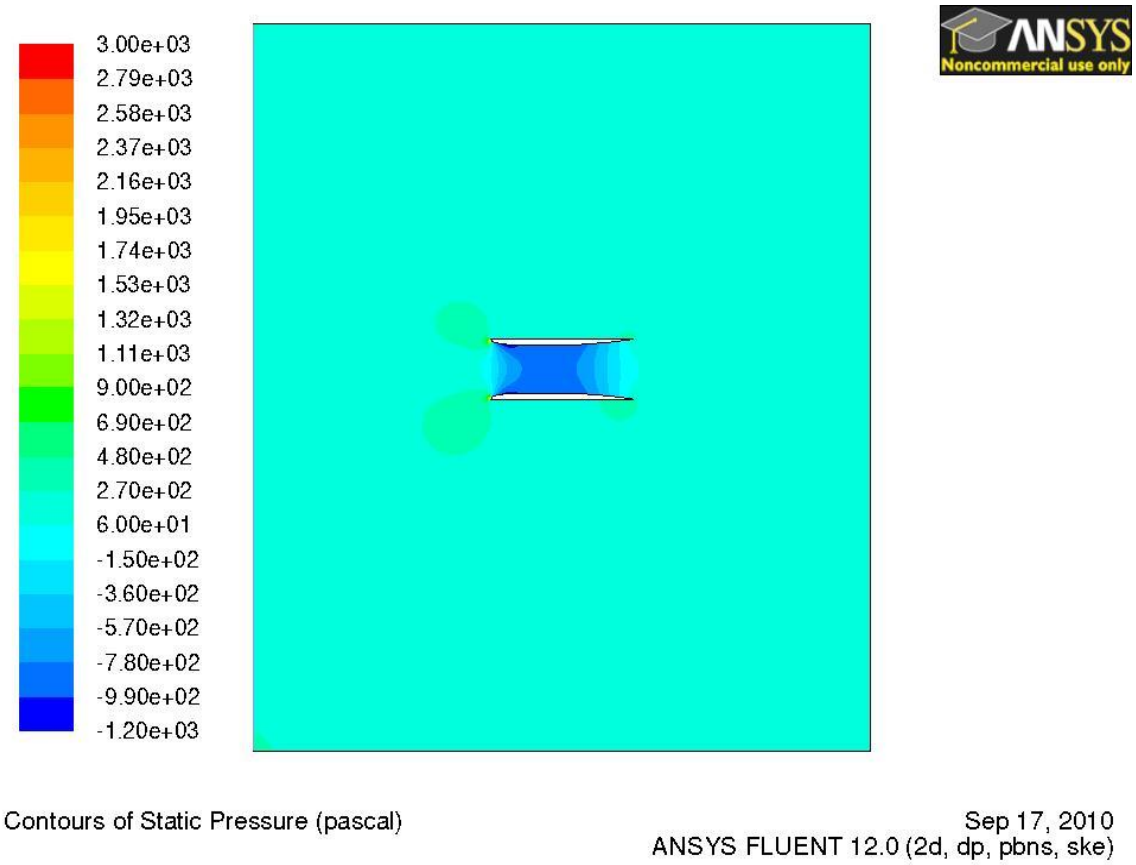

Figure 8.4 contour of pressure 6%t/c hydrofoils.

Three dimensional results show only a slightly different result to the 2D results because of the neglecting of two important characteristics of the actual flow situation. The calculation neglected the free surface effect which has a tendency to complicate the flow profile. In additional to neglecting the free surface effect, the bed roughness would also have an effect on the velocity profile.

	2D	3D		2D	3D		2D	3D
V_{in}	1	1	V_{in}	2	2	V_{in}	2.5	2.5
$V_{channel}$	1.834	1.7625	$V_{channel}$	3.663	3.22	$V_{channel}$	4.7507	4.236

Table 8.6 3D results compared with 2D results.

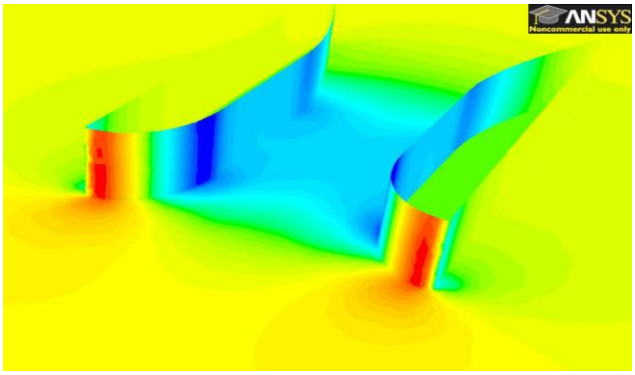

Figure 8.5 pressure contour of pressure
For a surface at one meter depth

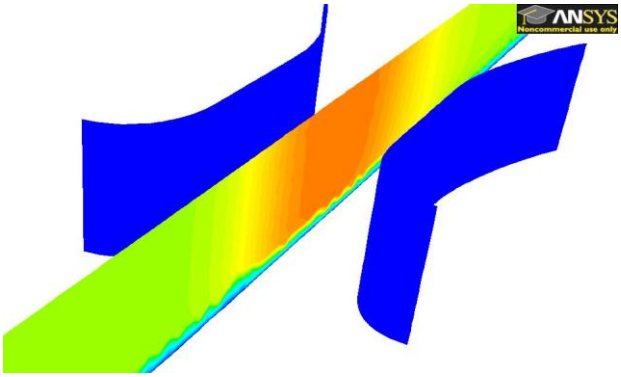

Figure 8.6 velocity contour
between the two hydrofoils

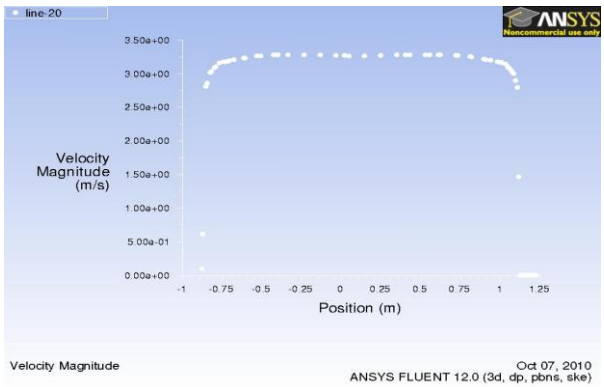

Figure 8.7 velocity profiles along the straight channel width at one meter depth

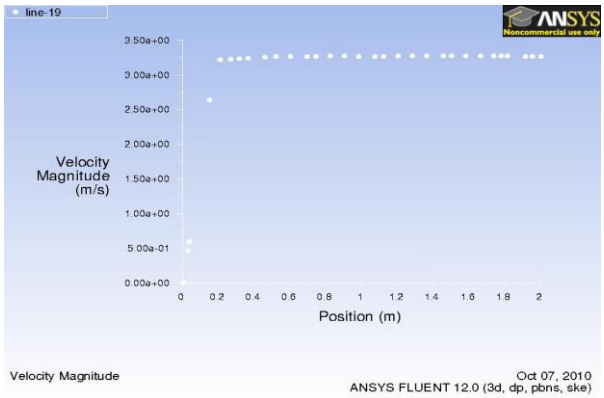

Figure 8 .8 velocity profile along channel depth in the medial of channel

In general, it is difficult to simulate flow in the cases that include rotating parts because of the complexity in flow structure. The complexity in flow in case including rotating parts is due to the high mean pressure and velocity gradient, the significantly amount of stream line curvatures, swirl flow and secondary flow.

Many error sources are expect to affect the results such as : cores grid, large time step, moving/static mesh treatment, turbulent model. Most of turbulent modeling shows weakness when they deal with cases includes large body forces as in rotating wheel case. Unfortunately there is no experimental data that we can compare our result with it.

The stationary blade test shows that the rectangular blade produces more torque in all in all three studied angles. The same conclusion is made from MRF results

stationary	45 deg	90 deg	135 deg
Triangular blades	31770 Nm	90712Nm	15620Nm
Rectangular blades	197702 Nm	93404Nm	51358Nm

Table 8.7 stationary blades torque

The results of tip speed ratio calculations and corresponding shaft power output for four triangular blades wheel at 2m/s inlet velocity are presented in table 8.8

Tip speed ratio	0.2	0.5	0.6	0.7	0.8	1
Shaft power (Kw)	1.15	2.3	2.36	2.525	2.352	1.66

Table 8.8 shaft power output at different tip speed ratio.

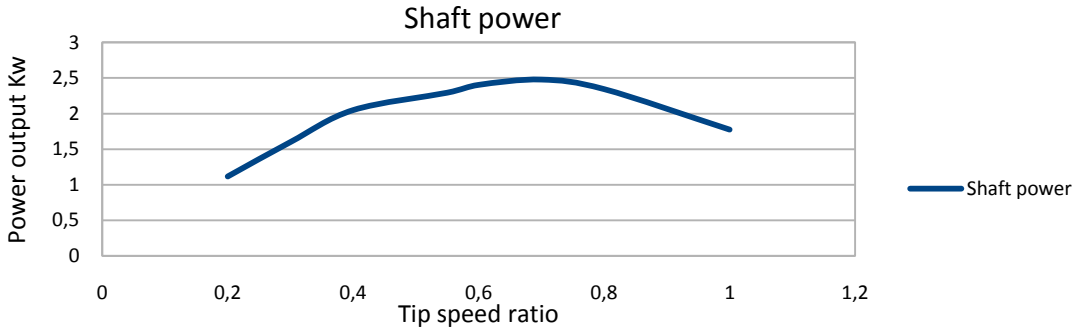

Figure 8.9 shaft power output at different tip speed ratio

Using eq-4.1 to calculate $P_{available}$ gives power available equal to 15.97kw.
Max power obtain from the four triangular blades at 0.7 tip speed ratio was 2.525Kw, which means that the max power coefficient from this type of waterwheel is$C_p = 0.16$
Output shaft power for wheel with four triangular blades is plotted against the rotational angle in figure 8.9

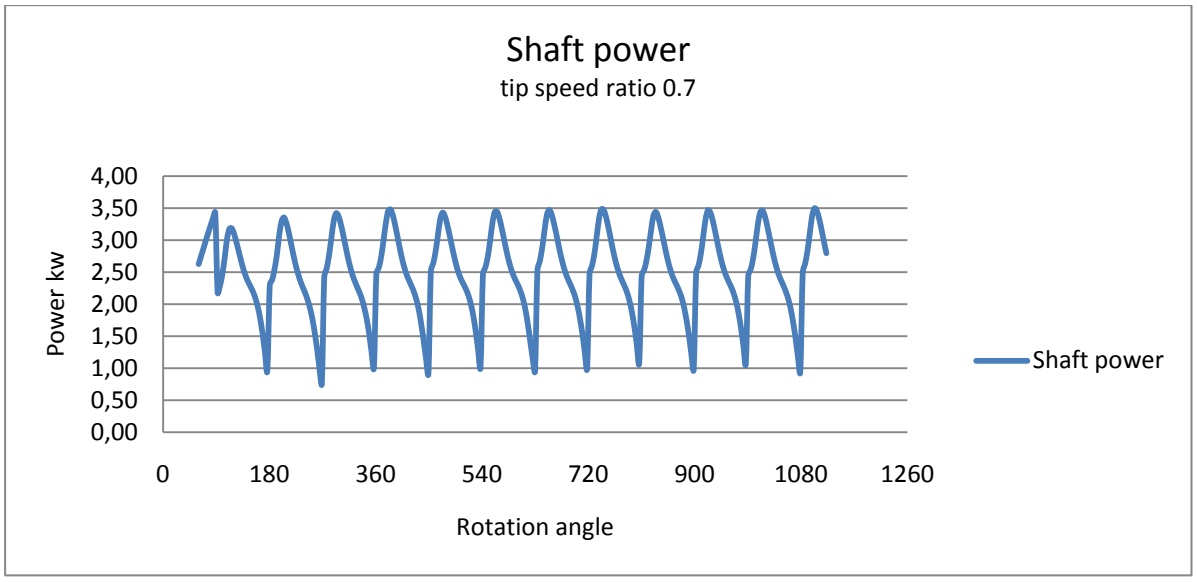

Figure 8.10output shaft powers for four triangular blades wheel rotating with 0.7 tip speed ratio

The power output results from the rectangular cases were compared with the triangular blade cases. Integrated power output for one revolution (360 deg) gives the power output 7.21kw and cp 0.45 at max efficiency which found to be also at 0.7 tip speed ratio.

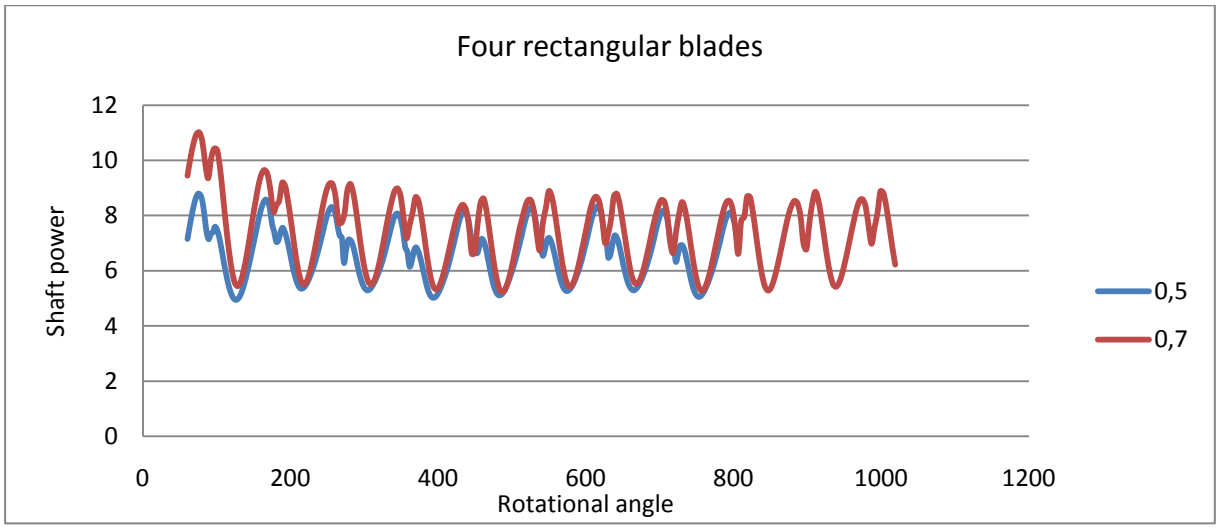

Figure 8.11 the result from four rectangular blades wheel at 0.5 and 0.7 tip speed ratios

Tip speed ratio curve was expected. The maximum efficiency at 0.7 tip speed ratio is also reasonable. The maximum efficiency can be at 0.5 tip speed ratio if all velocity vectors were parallel to each other and that the flow was receding at an 180deg angle. One more assumption is also required that there is no friction at blade surface. In practice the flow recede at different angles depending on blade geometry.

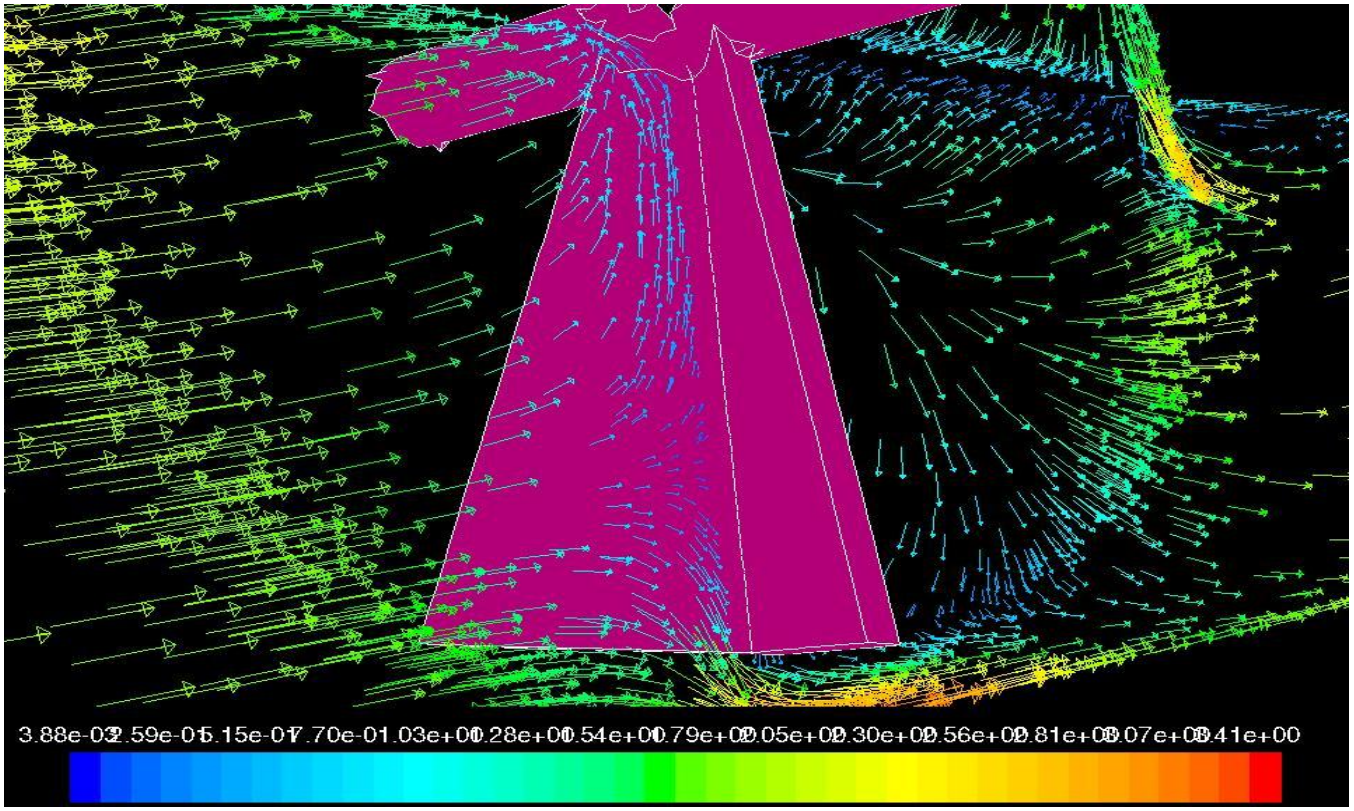

Figure 8.12 velocity vectors in triangular blades.

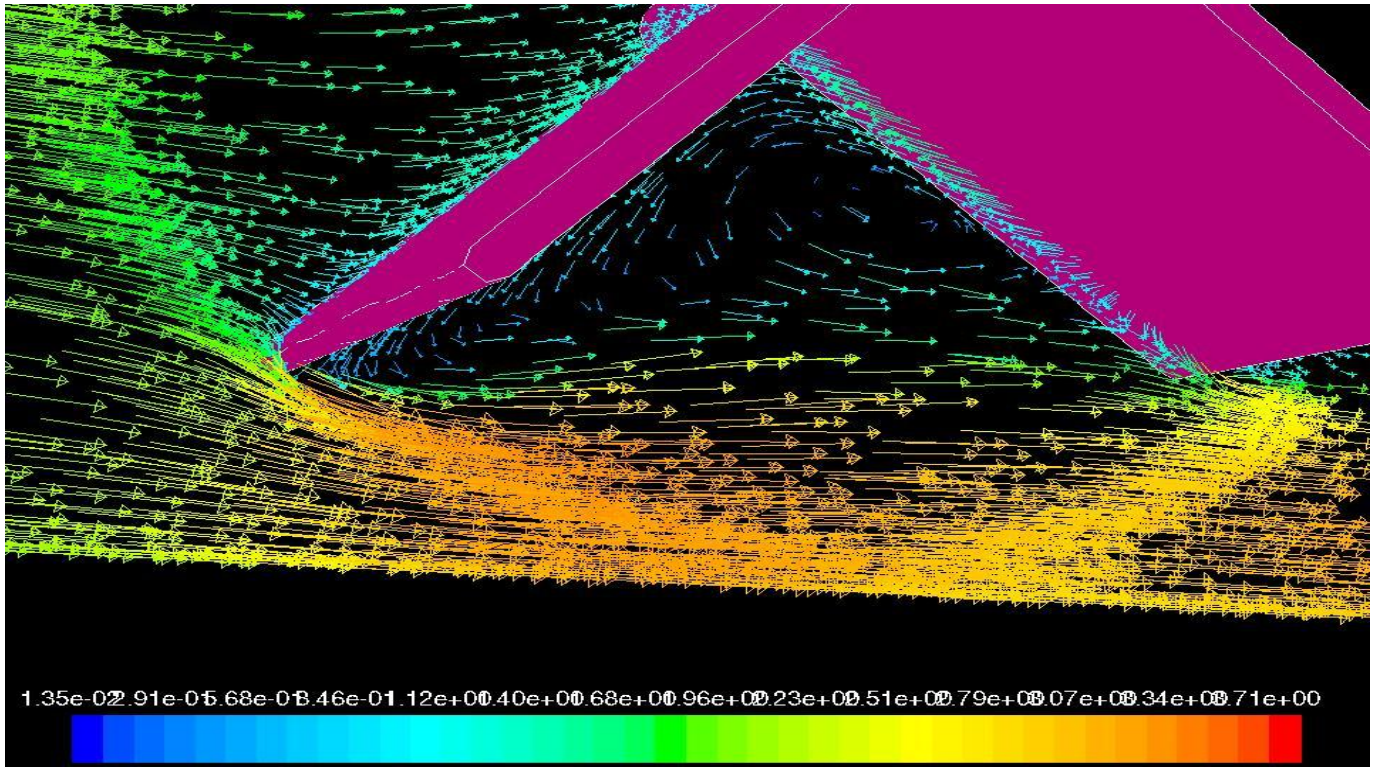

Figure 8.13 velocity vectors in rectangular blades.

The above vector plot shows how the flow recedes by different angles and the flow velocity is 3 dimensional. The triangular blade was proposed to reduce energy losses due to water resistance when the blade cuts the water surface. The result shows that the triangular blade inflict less drag due to its sharp edge, but at the same time the power output from the blade is reduced by about 30%. This reduction in power output is due to shrinkage of the wake behind the triangular blades. It is much smaller than the wake behind a rectangular blade. This causes a decrease in pressure difference between the two sides of the blade and a decrease in efficiency. The other reason that causes decrease in the power output in case of triangular blades is the leak of flow from the upper part of blade. The figure below shows this leak in flow.

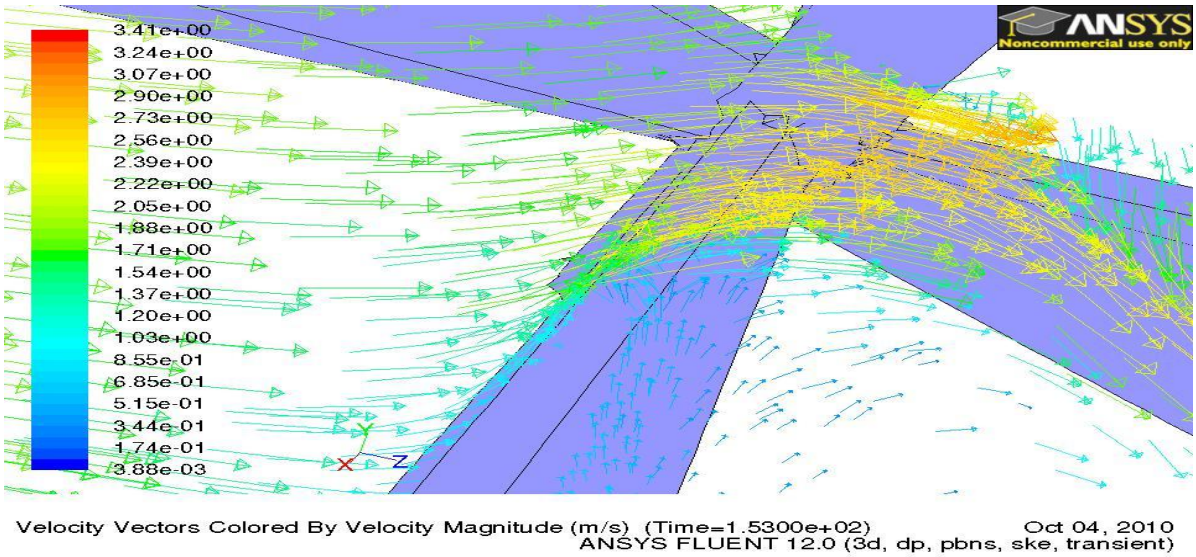

Figure 8.14 Velocity vector in triangular blade, the leak in flow

The velocity vector at two different depths in both rectangular and triangular shows how the flow conditions differed because of the flow leaks.

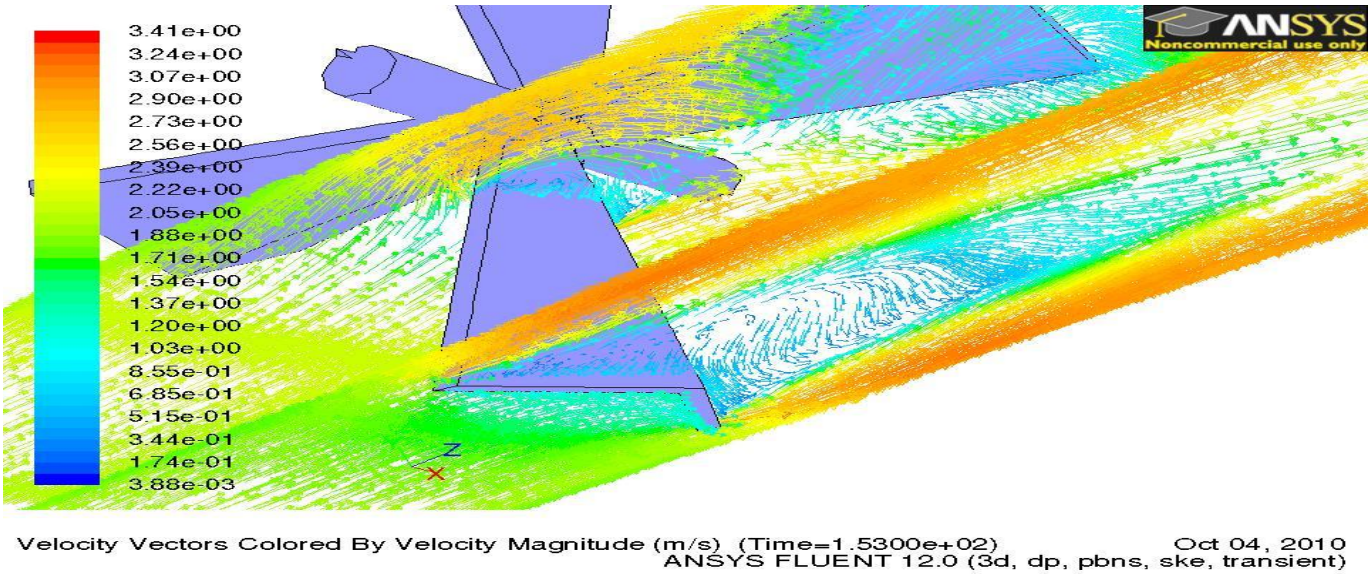

Figure 8.15 velocity vectors at different depth, triangular blades

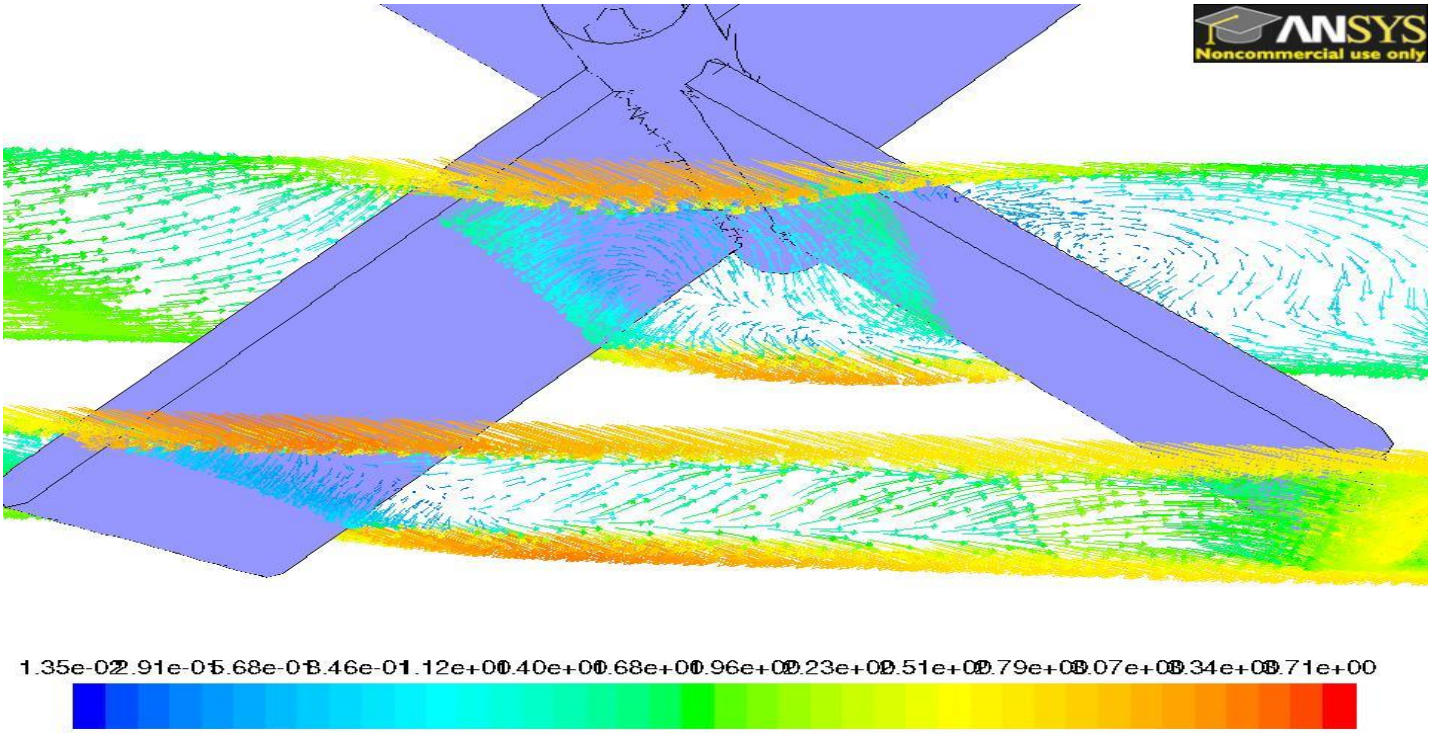

Figure 8.16 velocity vectors at different depth for rectangular blades

By using six blades instead of four blades the output power profile improved and the power output increased. Integrated power output for several rotations show that the shaft power is 10.56kw and the power coefficient is equal to 0.66.

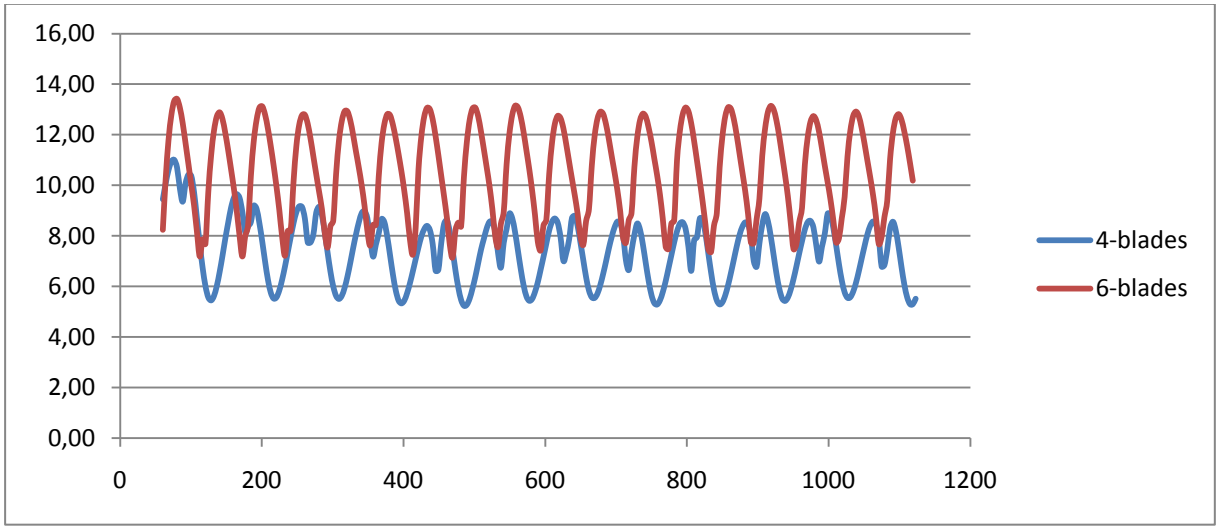

Figure 8.17 shaft output power for four and sig blade rectangular blades wheel at 0.7 tip speed ratio

The four blade result show that inside the water the rectangular blade need to be inclined with at least a 20 degree angle to start contributing to the torque. The blade contributes by producing torque until 135 degrees, after that the contribution becomes negative. That mean the blade will be active only for 115 degrees of the 180 degrees in the water. By adding more blades, more blades

contribute to the positive torque giving an improved efficiency. Even though the active angles are the same in both cases, in case of 6 blades there are always at least 2 blades contributing to the torque.

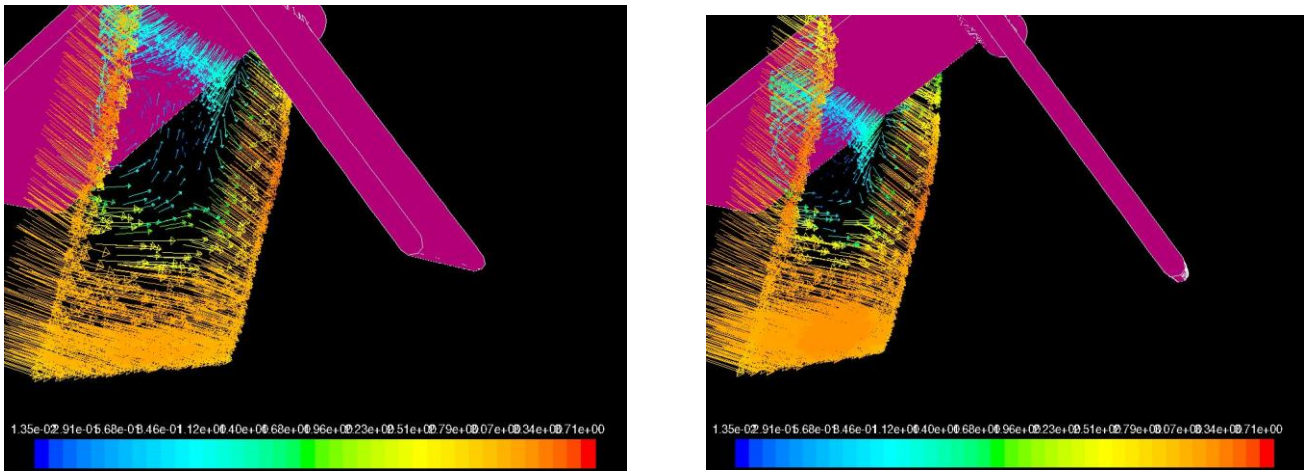

Figure 7.18 the wake flow behind the blade

9. Conclusion

The geometry of the channeling device was studied. Number of different geometrical parameters was introduced, which can be used to help at design similar channel for a different uses.

The suggested triangular blade show weak performance compared with rectangular blade (about 30% reduction in efficiency). But the water wheel shows a reasonable performance and also show potential for further improvement in future studies.

Since the stationary/moving mesh treatment is unavoidable, therefore these calculations can be improved by increase the mesh number and decrease the time steps. The use of non linear viscosity model which allow the calculation of secondary flow which cannot be solved by using k-epsilon model can also improve the results, Reynolds stress models can also be used since it shows successful in calculating strong swirl and stream line curvature. Reynolds- stress model required more computational time and recourses since it solve more equations.

Future work can be trying other types of blades and combined the CFD work with experimental works.

References

[1] Ren21. Renewable global status report, 2006

[2] U.S Department of energy 2010-10-05 http://www.energy.gov/

[3] Dixon, S. L. Fluid Mechanics and Thermodynamics of Turbomachinery (5th edn)

[4] Sornes, Kari Small Scale Water Current Turbine for River Applications. Zero Emission Resource Oranization, January 2010

[5] H K Versteg, W Malasakera, An introduction to Computational Fluid Dynamics The Finite Volume Method ,Pearson Education Limited, Essex ,England,1995

[6] S.B Pope, Turbulent Flows, Cambridge University Press, Cambridge, UK, 2001

[7] F.M White, Fluid Mechanics, 6th edn, McGraw-Hill, New York, 2008

[8] Fluent 12.0 User Guide, ANSYS, Electronic version, 2009-01-23

[9] H. chanson, The Hydraulics of Open Channel Flow: An Introduction (2nd edn)

[10] Md. Jahangir, M.T. Iqbal, Design and Development of Hybrid Vertical Axis Turbine, IEEE

[11] J.Zsnette, D. Imbault, A. Tourabi, A design methodology for cross flow water turbines , Renewable Energy 2009

[12] In Seong Hwang , oPtimization of cycloidal water turbine and the performance improvement by individual blade control, Applied Energy 86(2009)1532-1540

[13] F. Ponta, An improved vertical-axis water-current turbine incorporating a channeling device, Renewable Energy 20(2000)223-241

[14] Fluent 12.0 theory Guide, ANSYS, Electronic version, 2009-01-23

[15]H K Versteg, W Malasakera, An introduction to Computational Fluid Dynamics The Finite Volume Method ,Pearson Education Limited, Essex ,England,1995

[16]Bengt Sundén, Course material, Numerical Heat transfer MMV042, Division of heat transfer, Lund Institute of Technology, 2006